Spectroscopic Studies and Vibrational Analysis of Quinic Acid by Using DFT Calculations and the SQM Approach

Davide Romani[1], Silvia Antonia Brandán[2,*]

[1]*SST, Servicio sanitario della Toscana, Azienda USL Toscana SudEst di Grosseto, Via Cimabue, 109, 58100 Grosseto, Italia.*

[2]*Cátedra de Química General, Instituto de Química Inorgánica, Facultad de Bioquímica. Química y Farmacia, Universidad Nacional de Tucumán, Ayacucho 471, (4000) San Miguel de Tucumán, Tucumán, Argentina.*

ABSTRACT

Quinic acid has been completely characterized combining the experimental available FTIR, FT-Raman, ^{1}H- and ^{13}C-NMR, ultraviolet and ECD spectroscopies with the corresponding predicted by B3LYP/6-311++G** calculations. Two isomeric structures of quinic acid, named *C1* and *C2* were theoretically studied in gas phase and in aqueous solution by using the same level of theory. These structures differ in positions of carboxyl -OH in relation to hydroxy -OH of C-COOH group, hence, it group in *C1* is *Trans* while in *C2 Cis*. *C1* is most stable in gas phase but *C2* is most stable in solution showing, this latter isomer low solvation energy in aqueous solution. This difference could be attributed to the low volume expansion observed for *C2*, in relation to *C1*. The dipole moment values of both isomers decrease in solution. Here, some structural properties were studied in order to explain why *C2* is the only isomer present in the natural products. Thus, Mulliken, MK and NPA charges, bond orders, stabilization energies, molecular electrostatic potentials and topological properties cannot explain satisfactorily the presence of *C2* because *C1* reveal a higher stability in both media than *C1*. The frontier orbitals analyses reveal that *C1* is clearly most reactive than *C2* in both media justifying its higher solvation energy and volume expansion in solution while the differences in electrophilicity and nucleophilicity indexes for *C1* and *C2*, respectively could easily justify their different strong red and blue colorations in the mapped surfaces. Although very good correlations are observed for *C2* in both ^{1}H- and ^{13}C-NMR spectra its presence in the quinic acid only could be supported by the ultraviolet spectrum while the ECD spectra confirm the absolute configurations for both isomers, as was experimentally observed. For first time, the force fields, complete vibrational assignments and force constants for *C2* of quinic acid in both media are reported.

1. INTRODUCTION

Chemically, the quinic acid is known with the IUPAC name: (3R,5R)-1,3,4,5-tetrahydroxy cyclohexane-1-carboxylic acid and since long time its bacterial oxidation was reported by Rogoff [1]. Then, after 30 years ago, the isolation and identification of (–)-quinic acid as an unidentified major tea-component was studied by Sakata *et al* [2]. The structure of this acid was experimentally determined by Abell *et al* [3] while the ^{1}H- and ^{13}C-NMR spectra for some derivatives of that acid were later published [4]. Subsequent studies related to different quinic acid derivatives, such as caffeoylquinic acids, copper (II), oxovanadium (IV) and Al (III) complexes were then performed [5-16]. Different authors have observed important biological properties in the acid and in some of their derivatives [16-20] while recent studies described by He *et al* suggest that quinic acid and their derivatives may offer therapeutic benefit in ischemic retinopathies. This is a very important result taking into account that vision loss is the most important complication in patients with diabetes [18-20]. The quinic acid can be isolated from leaves of plants such as, cinchona bark, coffee beans, tobacco leaves, carrot leaves, apples, peaches, pears, plums, or can also be synthesized by hydrolysis of chlorogenic acid [21-25]. On the other hand, the chlorogenic acid can be synthesized from L-phenylalanine and quinic acid, as reported by Hanson and other authors [25-27]. So far, few vibrational studies were reported for quinic acid and its derivatives [11, 12, 16] and only some bands observed in the infrared and Raman spectra of this acid were identified by using the vibrational spectroscopy, for which, this acid cannot be completely identified with that technique. Hence, to perform the complete vibrational assignments by using the existent structure of quinic acid it is necessary first to study all possible isomers in order to find the structure that corresponds to the experimental one in order to predict the corresponding vibrational spectra. The quinic acid presents two asymmetric C atoms and two *Cis* or *Trans* isomers are expected when change the position of carboxyl -OH of COOH group. Knowing the most stable isomer, with the normal internal coordinates and by using known scale factors and with the Scaled Mechanical Quantum Force Field (SMQFF) methodology [28-29] both vibrational spectra can be assigned with the aid of Molvib program [30]. Here, the dimeric species of quinic acid was also considered because some intense bands observed in the experimental available IR and Raman spectra of acid in the solid phase can be easily justified by the presence of that structure of quinic acid. The force constants were also reported here. Additionally, taking into account that some derivatives of quinic acid were evaluated as potential biopesticides [31] while that other with pharmaceuticals, industrial, antioxidant and

Citation: Silvia Antonia Brandán et al. Ijsrm.Human, 2018; Vol. 11 (1): 25-56.

26

anti-carcinogens properties [32], the frontier orbitals and some descriptors were also reported because it is very important to predict the reactivities and behaviors of this acid in gas phase and in aqueous solution [33-35].

2. MATERIALS AND METHODS

2.1. Experimental IR, Raman, ^{1}H-NMR, ^{13}C-NMR, UV-visible and ECD spectra

The experimental available infrared and Raman spectra of quinic acid in the solid phase were taken from internet [36,37] while the experimentally available ultraviolet-visible and Electronic Circular Dichroism (ECD) spectrum of quinic acid were taken from Rogoff and Katzin, respectively [1,38]. The experimentally available ^{1}H- and ^{13}C-NMR spectra quinic acid in DMSO-d$_6$ and D$_2$O solutions were taken from internet [39-41].

2.2. Quantum mechanical calculations

The *GaussView* and Gaussian 09 Revision A.02 programs [42,43] were used to model and optimize the structures of quinic acid in gas phase and in aqueous solution by using the hybrid B3LYP/6-311++G** method [44,45]. Both monomer and dimer structures were taken from those experimental determined by X-ray diffraction where the cyclohexane ring in (-)-quinic acid is an almost perfect chair [3]. .The solvent effects and the optimizations in solution were carry out with the Integral Equation Formalism Variant Polarised Continuum Model (IEFPCM) model at the same level of theory [46,47] while the solvation energies was calculated by using the Solvation Model (SM) [48]. The volume variations that experiments the acid in the different media were calculated with the Moldraw program [49]. Two isomeric structures of quinic acid (*C1* and *C2*) were considered in this study, as can be seen in Fig.1, where in *C1* the position of hydroxy O5-H25 group that belong to COOH is *Trans* in relation to hydroxy O1-H21 group that belong to C-COOH. In *C2*, the hydroxy O5-H25 group is staggered in relation to the ring, with the hydroxy O5 atom directed towards the α side of the molecule, in *Cis* position, as in that experimental structure reported by Abell *et al.* (O7 with O1, see Fig. 1) [3]. Later, it is easy to see that the *C2* structure corresponds to that experimental perspective view of the structure of (-)-quinic acid (I) also presented in Fig. 1. Therefore, although *C2* is the only structure experimentally determined of quinic acid all properties studied in this work are presented for *C1* and *C2* in order to understand why the *C1* structure despite to have a minimum energy is not presents in the solid phase.

Citation: Silvia Antonia Brandán et al. Ijsrm.Human, 2018; Vol. 11 (1): 25-56.
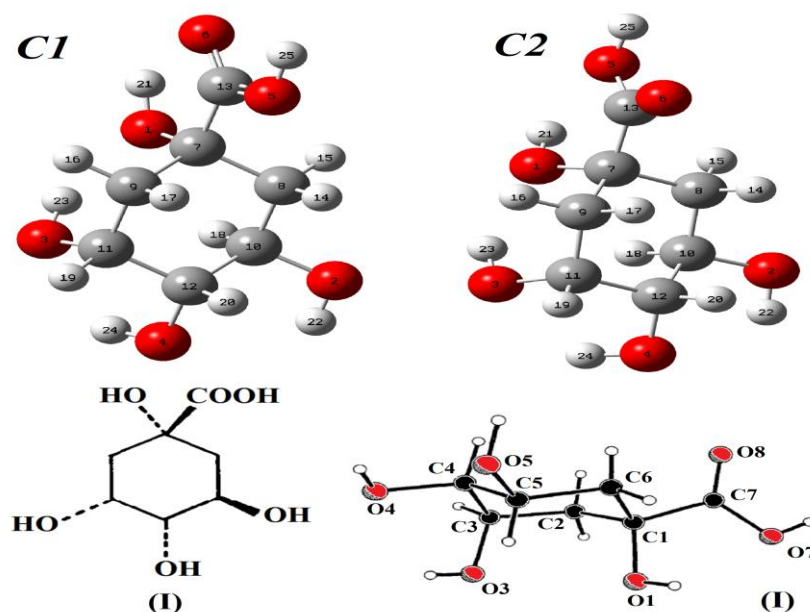
27

Fig. 1. Theoretical structures of *C1* and *C2* isomers of quinic acid with the atoms numbering together with a perspective view of the experimental X-ray structure for *C2*.

Then, the Natural Population Atomic (NPA) charges, bond orders (expressed as Wiberg indexes), Molecular Electrostatic Potentials (MEP), stabilization and solvation energies and topological properties were computed for those two structures by using the Merz-Kollman (MK) charges [50] and the NBO 5.1 and AIM2000 programs [51-53]. The harmonic force fields of *C1* and *C2* expressed in Cartesian coordinates and in both media were calculated with the SMQFF methodology [28] and the Molvib program [30]. The transformation of those force fields to internal coordinates were performed with the Molvib program [30] by using the normal internal coordinates and known scale factors [29] while the vibrational assignments of both experimental infrared and Raman spectra were completed with the transformed force fields and employing Potential Energy Distribution (PED) contributions $\geq$ 10 %. On the other hand, the predicted ^{1}H and ^{13}C-NMR spectra for *C1* and *C2* were computed with the Gauge-Independent Atomic Orbital (GIAO) method [54] using as reference tetramethylsilane (TMS). After that both spectra were compared with the corresponding experimental available ones [39-41]. The ultraviolet-visible spectrum and the rotatory strengths of quinic acid were also predicted in water using Time-dependent DFT calculations (TD-DFT) at the 6-311++G** level of theory. The comparisons of those predicted UV-visible and ECD spectra show good concordances with the corresponding experimental ones [1,38].

Citation: Silvia Antonia Brandán et al. Ijsrm.Human, 2018; Vol. 11 (1): 25-56.

28

3. RESULTS AND DISCUSSION

3.1. Stabilization energies in both media

In **Table 1** are presented the calculated total energies, dipole moments, volumes and corrected solvation energies by Zero Point Vibration Energy (ZPVE) for *C1* and *C2* of quinic acid in gas and aqueous solution phases and, by using the hybrid B3LYP/6-311++G** method. Two corrections should be performed in the solvation energies; one of them is by ZPVE and the other one by the total non-electrostatic terms.

Table 1. Calculated total energies (*E*), dipole moments (μ), volumes (V) and corrected solvation energies by zero point vibration energy of quinic acid (ΔG$_{un}$) in gas and aqueous solution phases.

B3LYP/6-311++G** Method					
Medium	E	ZPVE	μ (D)	V (Å^3)	ΔG$_{un}$
C1					
GAS	-725.5591	-725.3557	3.42	182.7	-49.05
PCM	-725.5888	-725.3370	5.70	184.0	
C2					
GAS	-725.5556	-725.3528	3.28	184.0	-9.44
PCM	-725.5909	-725.3492	4.36	184.5	

ΔG$_{un}$= uncorrected solvation energies by non-electrostatic terms

Examining the energy values we observed that *C1* is most stable in gas phase while *C2* in solution with energies differences between them of 9.18 and 5.51 kJ/mol in gas phase and solution, respectively without consider corrections by ZPVE while when the corrections are considered the energy values change to 7.60 and 32.0 kJ/mol, respectively. Probably, the high energy difference observed for *C1* in solution justify that this isomer is not present in natural form of the quinic acid. In Table 1 are observed the uncorrected terms (ΔG$_{un}$) because only the corrected solvation energy by ZPVE are presented in both media while both corrections, including those by the total non-electrostatic terms, are presented in **Table 2**. Hence, the corrected solvation energies (ΔG$_c$) are really obtained when both corrections are considered. In solution, the two isomers of quinic acid expand its volumes, as compared with the corresponding values in gas phase, showing higher values *C1* than *C2*. Hence, the final corrected solvation energy value is lower for *C2* than *C1*, as it is observed in Table 2.

Citation: Silvia Antonia Brandán et al. Ijsrm.Human, 2018; Vol. 11 (1): 25-56.

29

Table 2. Corrected and uncorrected solvation energies by the total non-electrostatic terms and by ZPVE for quinic acid by using the B3LYP/6-311++G** method.

B3LYP/6-311++G** method				
Solvation energy (kJ/mol)				ΔV (Å^3)
Condition	$\Delta G_u^{\#}$	ΔG_{ne}	ΔG_c	
C1				
Uncorrected	-77.90	22.36	-100.26	1.3
Corrected by	-49.05	22.36	-71.41	
C2				
Uncorrected	-92.59	21.32	-113.91	0.5
Corrected by	-9.44	21.32	-30.76	

$\Delta G_u^{\#}$= uncorrected solvation energy: defined as the difference between the total energies in aqueous solutions and the values in gas phase.

ΔG_{ne}= total non electrostatic terms: due to the cavitation, dispersion and repulsion energies.

ΔG_c= corrected solvation energies: defined as the difference between the uncorrected and non-electrostatic solvation energies.

On the other side, the dipole moment value only for *C1* increases from 3.42 D observed in gas phase to 5.70 D in solution while for *C2* decreases. Besides, we can see from **Fig 2** that the vector of dipole moment in solution for *C1* changes notably the magnitude, direction and orientation, as compared with that observed in gas phase while for *C2* only a change in the magnitude of dipole moment in solution is observed. These variations could explain the low solvation energy observed for *C2*. Obviously, the presence of OH groups in both structures with different characteristics and different hydration's types with water molecules could justify the differences between both isomers.

3.2. Geometrical parameters in both media

Calculated geometrical parameters for both stable *C1* and *C2* isomers of quinic acid in gas and aqueous solution phases by using the B3LYP/6-311++G** method are summarized in **Table 3** compared with the corresponding experimental ones determined by Abell *et al.* for (-)-quinic acid in the solid-state [3]. The evaluations of the differences between theoretical and experimental values were performed by using the Root Mean Square Deviation (RMSD) values which are presented in the same table.

Citation: Silvia Antonia Brandán et al. Ijsrm.Human, 2018; Vol. 11 (1): 25-56.
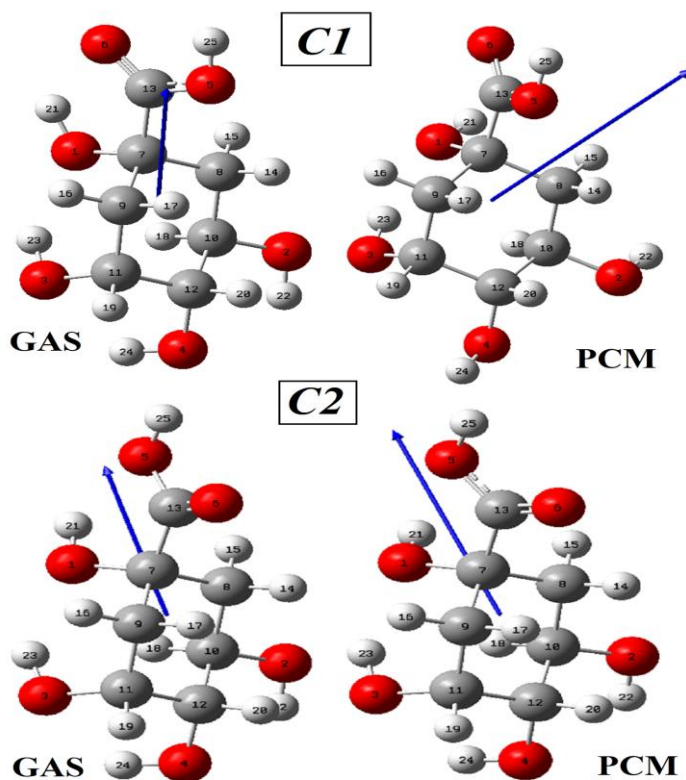
30

Fig 2. Magnitudes and orientations of dipole moments vectors of *C1* and *C2* isomers of quinic acid in gas phase and in aqueous solution by using the B3LYP/6-311++G** level of theory.

Both, *C1* and *C2* isomers demonstrate good concordances in the bond lengths and angles in the two media with values for bond lengths between 0.019 and 0.014 Å and between 2.1 and 1.6º for bond angles. Note that *C2* presents the lower bond lengths and angles values in solution because, as we observed before, it is the most stable conformation in this medium. The evaluation exhaustive of that table shows clearly that the C13=O6 bonds corresponding to -COOH group are predicted in both conformations with double bonds characters while the other C13-O5 bonds of same groups are predicted with partial double bonds characters. In solution, the C13=O6 bonds are slightly elongated as compared with the C13-O5 bonds, as expected because the O6 atoms have lone pairs that can form H bonds with water molecules.

Citation: Silvia Antonia Brandán et al. Ijsrm.Human, 2018; Vol. 11 (1): 25-56.

31

Table 3. Comparison of calculated geometrical parameters for *C1* and *C2* of quinic acid in both media with the corresponding experimental ones.

B3LYP/6-311++G** Method [a]					Experimental[b]
Parameter	*C1*		*C2*		
	Gas	PCM	Gas	PCM	
Bond lengths (Å)					
C7-C8	1.542	1.542	1,546	1,543	1.528(3)
C7-C9	1.546	1.539	1,536	1,539	1.541(3)
C7-C13	1.527	1.536	1,534	1,536	1.525(2)
C8-10	1.527	1.534	1,527	1,526	1.517(3)
C10-C12	1.532	1.523	1,531	1,531	1.516(3)
C12-C11	1.538	1.543	1,536	1,537	1.517(3)
C9-C11	1.533	1.532	1,532	1,530	1.521(3)
C7-O1	1.432	1.432	1,437	1,433	1.417(2)
C10-O2	1.424	1.437	1,423	1,436	1.431(2)
C12-O4	1.424	1.432	1,424	1,433	1.440(2)
C11-O3	1.431	1.436	1,433	1,440	1.438(2)
C13-O5	1.342	1.340	1,356	1,339	1.306(3)
C13=O6	1.208	1.213	1,201	1,215	1.216(3)
RMSD[b]	**0.015**	**0.015**	**0.019**	**0.014**	
Bond angles (°)					
C8-C7-C9	110.5	110.6	110,8	110,7	110.8(2)
C8-C7-C13	110.7	109.0	107,8	108,0	108.5(1)
C8-C7-O1	109.0	110.8	110,9	111,0	107.9(1)
C9-C7-C13	110.4	111.1	110,3	109,1	106.7(1)
C9-C7-O1	108.7	106.6	106,3	106,5	111.0(1)
C13-C7-O1	107.3	108.4	110,6	111,2	111.9(1)
C7-C8-C10	110.5	112.5	111,1	111,5	114.4(1)
C8-C10-C12	111.5	110.7	111,4	111,4	110.9(1)
C8-C10-O2	107.6	109.8	107,6	107,2	108.5(1)
C12-C10-O2	110.6	108.1	110,8	110,8	111.1(1)
C10-C12-C11	112.3	111.7	112,0	112,2	111.0(2)
C10-C12-O4	110.0	108.5	109,9	110,5	106.6(1)
C11-C12-O4	110.7	111.4	110,8	110,8	113.5(1)
C12-C11-C9	111.1	110.7	111,3	111,1	109.5(1)
C12-C11-O3	110.0	112.2	109,7	110,6	110.5(1)
C9-C11-O3	113.0	112.2	113,3	112,6	111.9(1)
C11-C9-C7	111.7	111.9	112,6	112,3	111.3(1)
C7-C13-O5	113.5	112.9	111,3	113,6	113.9(2)
C7-C13=O6	122.9	123.9	125,5	123,2	122.3(2)
O6=C13-O5	123.5	123.1	123,0	123,0	123.8(2)
RMSD[b]	**2.1**	**2.1**	**1.7**	**1.6**	
Dihedral angles (°)					
C9-C7-C8-C10	57.1	53.9	55,2	54,9	-49.0(2)
C7-C8-C10-	-56.5	-54.8	-56,0	-55,3	50.8(2)
C8-C10-C12-C11	54.6	55.5	55,2	54,7	-56.3(2)

Citation: Silvia Antonia Brandán et al. Ijsrm.Human, 2018; Vol. 11 (1): 25-56.

32

C10-C12-C11-	-52.8	-56.0	-53,1	-53,5	61.0(2)
C12-C11-C9-	53.7	55.3	52,9	53,5	-59.2(2)
C11-C9-C7-C8	-56.2	-54.1	-53,9	-54,3	52.8(2)
O1-C7-C13-O5	-179.7	170.3	-31,5	-10,0	-8.3(2)
O5-C13-C7-C8	-60.8	-68.7	89,9	112,1	
O5-C13-C7-C9	61.8	53.4	-	-127,2	
C13-C7-C9-C8	-122.8	-121.31	-	-118,9	-127.3(2)
RMSD[b]	**112.9**	**114.2**	**95.0**	**94.7**	

[a]This work, [b]Ref [3]

In relation to the dihedral angles we observed that *C2* presents the lowest RMSD values in the two media, as compared with *C1*. On the other side, when the O1---O6 and O1---O5 distances between the most electronegative atoms of the -COOH groups together with the O---H distances of H bonds for *C1* and *C2* in both media, respectively are evaluated from **Table 4**, clearly it is observed the lower value in the O1---O5 distance (2.631 Å) for *C2* could probably justify a higher repulsion between the two O atoms and, for this reasons, this isomer will be unstable and presents higher energy and higher length in the O5---H21 bond (2.227 Å), as compared with *C1*. Hence, the presence of C2 in the solid state is easily justified because this form is the only experimentally observed by X-ray diffraction.

Table 4. Calculated O---O and O---H distances (Å) for both conformations of quinic acid by using the B3LYP/6-311++G** method in gas phase and in aqueous solution.

Distances	*C1*		*C2*	
	Gas	PCM	Gas	PCM
O1---O6	2.635	2.699		
O1---O5			2.631	2.605
O6---H21	2.033	2.665		
O5---H21			2.227	2.606

3.3. Charges, bond orders and MEP studies

For *C1* and *C2* of quinic acid in both media, Mulliken, MK and NPA charges, bond orders and molecular electrostatic potentials were examined by using B3LYP/6-311++G** level of theory and different programs calculations [50-53]. All these results can be observed in **Table 5** while variations in Mulliken, MK and NPA charges for *C1* and *C2* in both media are represented respectively in **Fig 3**.

Citation: Silvia Antonia Brandán et al. Ijsrm.Human, 2018; Vol. 11 (1): 25-56.

33

Table 5. Mulliken, Merz-Kollman and NPA charges, MEP and bond orders, expressed as Wiberg indexes for both forms of quinic acid in gas phase and in aqueous solution by using B3LYP/6-311++G** calculations.

C1

Atoms	GAS					PCM				
	MK	Mulliken	NPA	MEP	BO	MK	Mulliken	NPA	MEP	BO
1 O	-	-0.240	-	-	1.787	-	-0.200	-	-	1.826
2 O	-	-0.192	-	-	1.803	-	-0.183	-	-	1.818
3 O	-	-0.216	-	-	1.795	-	-0.152	-	-	1.808
4 O	-	-0.195	-	-	1.804	-	-0.175	-	-	1.827
5 O	-	-0.136	-	-	2.004	-	-0.147	-	-	1.992
6 O	-	-0.237	-	-	2.027	-	-0.240	-	-	2.034
7 C	0.224	-0.062	0.188	-	3.941	0.489	0.019	0.190	-	3.939
8 C	-	-0.193	-	-	3.933	-	-0.491	-	-	3.937
9 C	-	-0.590	-	-	3.927	-	-0.819	-	-	3.926
10 C	0.399	-0.358	0.105	-	3.903	0.772	-0.275	0.110	-	3.901
11 C	0.359	0.026	0.104	-	3.901	0.571	-0.002	0.108	-	3.916
12 C	0.110	-0.691	0.085	-	3.904	-	-0.337	0.096	-	3.911
13 C	0.679	0.134	0.805	-	3.834	0.736	0.128	0.793	-	3.842
14 H	0.081	0.214	0.223	-1.100	0.953	0.195	0.231	0.230	-1.091	0.951
15 H	0.096	0.216	0.225	-1.103	0.952	0.157	0.189	0.201	-1.085	0.963
16 H	0.185	0.238	0.222	-1.093	0.954	0.208	0.251	0.231	-1.098	0.950
17 H	0.137	0.169	0.227	-1.088	0.951	0.151	0.182	0.228	-1.092	0.951
18 H	-	0.256	0.172	-1.119	0.975	-	0.253	0.178	-1.108	0.973
19 H	0.061	0.252	0.190	-1.109	0.969	0.019	0.223	0.180	-1.110	0.971
20 H	0.075	0.236	0.186	-1.108	0.969	0.081	0.208	0.168	-1.109	0.976
21 H	0.418	0.290	0.498	-0.973	0.757	0.416	0.288	0.475	-0.969	0.779
22 H	0.415	0.244	0.473	-1.005	0.781	0.385	0.240	0.453	-0.995	0.799
23 H	0.435	0.261	0.489	-0.999	0.765	0.458	0.251	0.479	-1.015	0.776
24 H	0.404	0.265	0.475	-1.001	0.779	0.416	0.248	0.455	-1.004	0.798
25 H	0.436	0.310	0.491	-0.922	0.764	0.427	0.309	0.491	-0.929	0.763

C2

Atoms	GAS					PCM				
	MK	Mulliken	NPA	MEP	BO	MK	Mulliken	NPA	MEP	BO
1 O	-	-0.226	-	-	1.798	-	-0.198	-	-	1.818
2 O	-	-0.192	-	-	1.803	-	-0.186	-	-	1.800
3 O	-	-0.221	-	-	1.795	-	-0.215	-	-	1.794
4 O	-	-0.196	-	-	1.803	-	-0.198	-	-	1.806
5 O	-	-0.173	-	-	1.970	-	-0.116	-	-	2.008
6 O	-	-0.232	-	-	2.050	-	-0.243	-	-	2.021
7 C	0.302	0.098	0.191	-	3.936	0.317	0.343	0.191	-	3.936
8 C	-	-0.017	-	-	3.932	-	-0.275	-	-	3.930
9 C	-	-0.862	-	-	3.924	-	-0.822	-	-	3.923
10 C	0.424	-0.294	0.107	-	3.906	0.380	-0.202	0.106	-	3.909
11 C	0.304	0.122	0.104	-	3.899	0.347	0.137	0.104	-	3.901
12 C	0.075	-0.754	0.085	-	3.904	0.146	-0.726	0.084	-	3.904

Citation: Silvia Antonia Brandán et al. Ijsrm.Human, 2018; Vol. 11 (1): 25-56.

34

13	C	0.698	-0.036	0.801	-14.616	3.839	0.673	-0.225	0.794	-14.621	3.844
14	H	0.084	0.226	0.225	-1.095	0.953	0.089	0.242	0.237	-1.094	0.947
15	H	0.091	0.194	0.220	-1.096	0.955	0.070	0.197	0.213	-1.091	0.958
16	H	0.193	0.254	0.228	-1.098	0.951	0.170	0.249	0.228	-1.097	0.951
17	H	0.130	0.195	0.238	-1.093	0.946	0.096	0.191	0.237	-1.092	0.947
18	H	-	0.238	0.166	-1.116	0.977	-	0.223	0.161	-1.106	0.980
19	H	0.083	0.252	0.191	-1.110	0.968	0.053	0.254	0.194	-1.109	0.967
20	H	0.088	0.233	0.188	-1.107	0.969	0.066	0.238	0.192	-1.104	0.967
21	H	0.432	0.321	0.486	-0.966	0.768	0.402	0.291	0.473	-0.964	0.780
22	H	0.419	0.248	0.474	-1.003	0.780	0.405	0.245	0.473	-0.999	0.781
23	H	0.430	0.261	0.487	-0.998	0.767	0.399	0.257	0.482	-1.000	0.772
24	H	0.401	0.265	0.476	-1.000	0.779	0.390	0.262	0.471	-0.999	0.784
25	H	0.452	0.297	0.494	-0.926	0.761	0.451	0.276	0.491	-0.931	0.764

Evaluating first the three charges on all atoms of *C1* we observed the higher differences mainly on the C atoms, in particular on the C7, C10 and C13 atoms are observed positive MK charges, however, on the C8, C9 and C12 atoms negative charges are observed. The NPA charges show the same behaviours in both media.
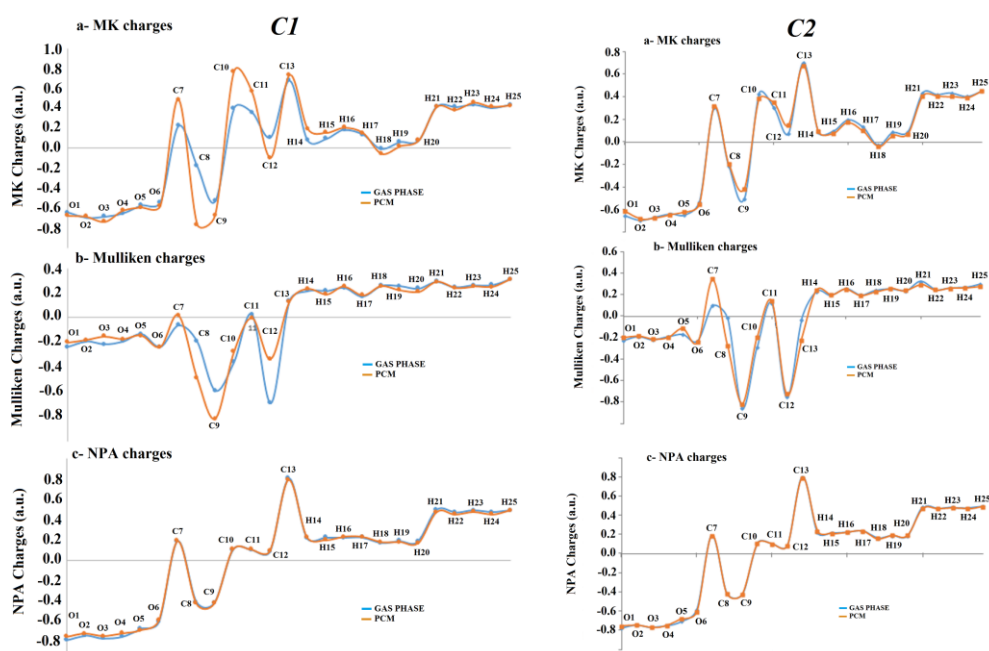

Figure 3. Comparisons of Mulliken, MK and NPA charges of *C1* and *C2* isomers of quinic acid in gas phase and in aqueous solution by using the B3LYP/6-311++G** level of theory.

Citation: Silvia Antonia Brandán et al. Ijsrm.Human, 2018; Vol. 11 (1): 25-56.

35

All charges on the H atoms practically do not show differences in solution, in relation to the values in gas phase. Here, negative NPA charges values are observed only on C8 and C9 while negative Mulliken charges are also observed on C8, C9, C10 and C12. For *C2* in both media, the MK and NPA charges on C12 are positive while the Mulliken charges on these atoms in the two media are negative and have practically the same values, different from *C1* where the charges on C12 present higher value in gas phase. When the three charges studied are analyzed on the O atoms in both media, the higher values are observed on the Mulliken charges while the MK and NPA charges show different behaviours for *C1*, but *C2* in solution reveals the same variation than *C1*.

Particularly, the studies related to MEP are interesting properties useful to predict the different nucleophilic and electrophilic reactions sites in all species and, in particular, the mapped surfaces allow finding those places observing simply the different colorations on the same. Thus, red colours are generated on nucleophilic sites while blue colours are on electrophilic ones. On the contrary, green colours are characteristics of inert regions. For *C1* and *C2*, the MEP values are summarized in Table 5 while in **Fig 4** are observed the mapped surfaces showing clearly the different colorations. For *C1* and *C2*, the red colours are observed on the O atoms of both -COOH and -OH groups while the blue colours on the H atoms of hydroxyl -OH groups. Hence, nucleophilic and electrophilic sites are clearly identified in both species where visibly these two isomers in solution show strong colorations not observed in gas phase. These results can be easily explained taking into account the different hydrations of both isomers in solution.

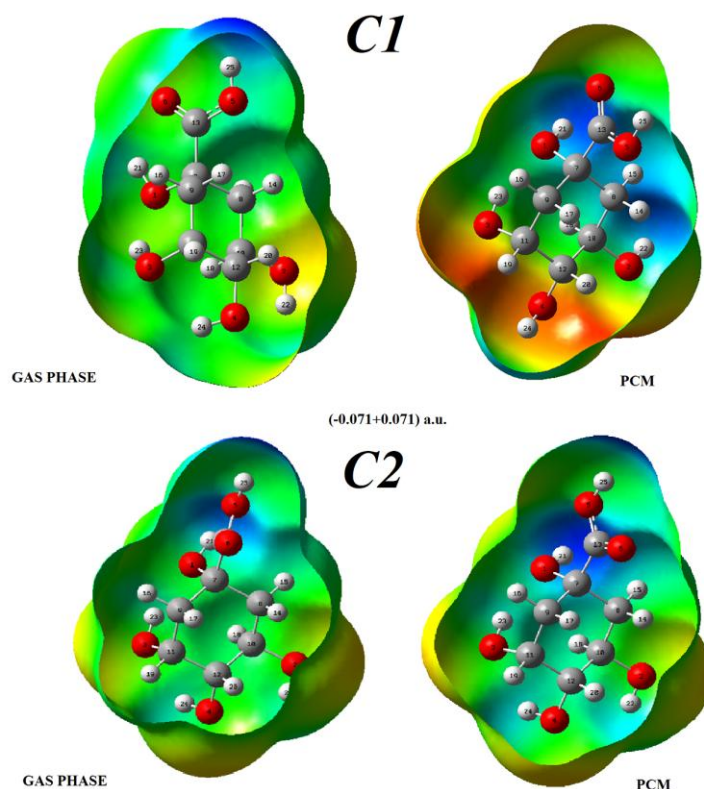*Citation: Silvia Antonia Brandán et al. Ijsrm.Human, 2018; Vol. 11 (1): 25-56.*

36

Figure 4. Calculated molecular electrostatic potentials on the mapped surfaces of *C1* and *C2* isomers of quinic acid in gas phase and in aqueous solution. Color ranges, in au: from red -0.071 to blue +0.071. B3LYP functional and 6-31G* basis set. Isodensity value of 0.005.

In Table 5 are also presented the total by atom Bond Orders (BO), expressed as Wiberg indexes for *C1* and *C2*. This property allow to us to know the type of bond formed between two atoms. Hence, analysing that table we observed that both O6 atoms belonging to -COOH groups present the higher BO values because these have double bonds characters while the O5 atoms belonging to -OH groups of -COOH groups show partial double bonds characters. On the other hand, the most labile H atoms, these implies the less bonded, are those observed in H21 and H25 where the former belong to -COOH and the second one to -OH groups closer to these groups in both isomers of quinic acid. These results are in complete agreement with the blue colours observed on the corresponding MEP surfaces.

3.4. NBO and AIM studies

The stabilities of *C1* and *C2* can be easily predicted calculating the main donor-acceptor energy interactions and their topological properties, as suggested by Bader for different

Citation: Silvia Antonia Brandán et al. Ijsrm.Human, 2018; Vol. 11 (1): 25-56.

37

species [53]. Thus, for both isomers of quinic acid in gas phase and in aqueous solution by using B3LYP/6-311++G** level of theory and the NBO and AIM programs [51,52] were calculated those properties which are presented in **Table 6**. Evaluating that table it is observed three similar interactions from lone pairs of O5 and O6 atoms toward anti-bonding orbitals $\pi^*O6\text{-}C13$, $\sigma^*O5\text{-}C13$ and $\sigma^*C7\text{-}C13$. The total energy values show clearly that *C1* in both media present values slightly higher than *C2*, for which, the *C1* forms are most stable than the *C2* ones and, for these reasons, this study cannot justify the presence of *C2* in the solid phase.

Table 6. Main delocalization energies (in kJ/mol) for both forms of quinic acid in gas and aqueous solution phases and by using B3LYP/6-311++G calculations.**

C1[a]		
Delocalization	B3LYP/6311++G**	
	Gas	PCM
$LP(2)O5 \rightarrow \pi^*O6\text{-}C13$	195.08	191.86
$\Sigma_{LP \rightarrow \sigma^*}$	**195.08**	**191.86**
$LP(2)O6 \rightarrow \sigma^*O5\text{-}C13$	131.33	131.33
$LP(2)O6 \rightarrow \sigma^*C7\text{-}C13$	71.81	76.91
$\Sigma_{LP \rightarrow \pi^*}$	**203.14**	**208.24**
Σ_{TOTAL}	**398.22**	**400.10**
C2[a]		
Delocalization	B3LYP/6311++G**	
	Gas	PCM
$LP(2)O5 \rightarrow \pi^*O6\text{-}C13$	153.19	188.35
$\Sigma_{LP \rightarrow \sigma^*}$	**153.19**	**188.35**
$LP(2)O6 \rightarrow \sigma^*O5\text{-}C13$	144.25	131.75
$LP(2)O6 \rightarrow \sigma^*C7\text{-}C13$	77.54	74.19
$\Sigma_{LP \rightarrow \pi^*}$	**221.79**	**205.94**
Σ_{TOTAL}	**374.98**	**394.29**

[a]This work

The Bader's theory [53] is also useful to investigate different characteristics in inter- and intra-molecular interactions by using the topological properties and the AIM2000 program [52]. Therefore, the electron density, $\rho(r)$, the Laplacian values, $\nabla^2\rho(r)$, the eigenvalues $(\lambda 1, \lambda 2, \lambda 3)$ of the Hessian matrix and, the $|\lambda 1|/\lambda 3$ ratio were calculated for *C1* and *C2* in the Bond Critical Points (BCPs) and in the Ring Critical Points (RCPs). The corresponding values of these properties can be seen in **Table 7** while in **Fig 5** are graphed the new interactions formed for both isomers in gas phase together with the related BCPs and RCPs.

Citation: Silvia Antonia Brandán et al. Ijsrm.Human, 2018; Vol. 11 (1): 25-56.

38

Table 7. Analysis of the BCPs and RCPs for both forms of quinic acid in gas and aqueous solution phases and by using the B3LYP/6-311++G method.**

B3LYP/6-311++G** Method					
C1					
GAS PHASE					
Parameter[#]	O1---H23	RCPN1	O6---H21	RCPN2	RCP
$\rho(r)$	0.0238	0.0135	0.0249	0.0245	0.0183
$\nabla^2\rho(r)$	0.0893	0.0708	0.1061	0.1284	0.1109
$\lambda 1$	-0.0308	-0.0100	-0.0289	-0.0260	-0.0160
$\lambda 2$	-0.0293	0.0343	-0.0141	0.0169	0.0629
$\lambda 3$	0.1494	0.0464	0.1492	0.1374	0.0639
$|\lambda 1|/\lambda 3$	0.2062	0.2155	0.1937	0.1892	0.2504
Distances	1.985			2.033	
AQUEOUS SOLUTION					
Parameter[#]	O1---H23	RCPN1	O6-H21	RCPN2	RCP
$\rho(r)$	0.0250	0.0138			0.0182
$\nabla^2\rho(r)$	0.0927	0.0726			0.1108
$\lambda 1$	-0.0325	-0.0102			-0.0157
$\lambda 2$	-0.0310	0.0350			0.0603
$\lambda 3$	0.1562	0.0477			0.0663
$|\lambda 1|/\lambda 3$	0.2081	0.2138			0.2368
Distances	1.974				
C2					
GAS PHASE					
Parameter[#]	O1---H23	RCPN1	O6---H21	RCPN2	RCP
$\rho(r)$	0.0217	0.0128			0.0182
$\nabla^2\rho(r)$	0.0836	0.0678			0.1109
$\lambda 1$	-0.0272	-0.0091			-0.0159
$\lambda 2$	-0.0256	0.0316			0.0624
$\lambda 3$	0.1365	0.0452			0.0644
$|\lambda 1|/\lambda 3$	0.1875	0.2013			0.2469
Distances	2.016				
AQUEOUS SOLUTION					
Parameter[#]	O1---H23	RCPN1	O6-H21	RCPN2	RCP
$\rho(r)$	0.0239	0.0136			0.0182
$\nabla^2\rho(r)$	0.0874	0.0705			0.1110
$\lambda 1$	-0.0306	-0.0101			-0.0159
$\lambda 2$	-0.0292	0.0337			0.0624
$\lambda 3$	0.1472	0.0468			0.0645
$|\lambda 1|/\lambda 3$	0.2079	0.2158			0.2465
Distances	1.997				

Citation: Silvia Antonia Brandán et al. Ijsrm.Human, 2018; Vol. 11 (1): 25-56.

39

Here, it is necessary to clarify that when the values of $|\lambda 1|/\lambda 3 < 1$ and $\nabla^2 \rho(r) > 0$ the interaction is typical of hydrogen bonds or ionic (closed-shell interaction) while when an interaction present high values of $\rho(r)$ and $\nabla^2 \rho(r)$, the ratio $\lambda 1/\lambda 3 > 1$ and $\nabla^2 \rho(r) < 0$ the interaction is covalent (shared interaction) [55]. *C1* shows two new H bonds, O1---H23 and O6---H21, and hence, appear two new RCPN1 and RCPN2, as shown in Fig. 6 while only the interaction O1---H23 is observed in *C2* together with its corresponding RCPN1. Obviously, in both isomers of quinic acid the cyclohexane rings present its own RCPs. Then, evaluating the number of H bonds formed, the distances between the atoms involved and the densities values, *C1* in both media are clearly most stable than *C2*. In this case, the presence of *C2* in the solid phase cannot be explained with this study.
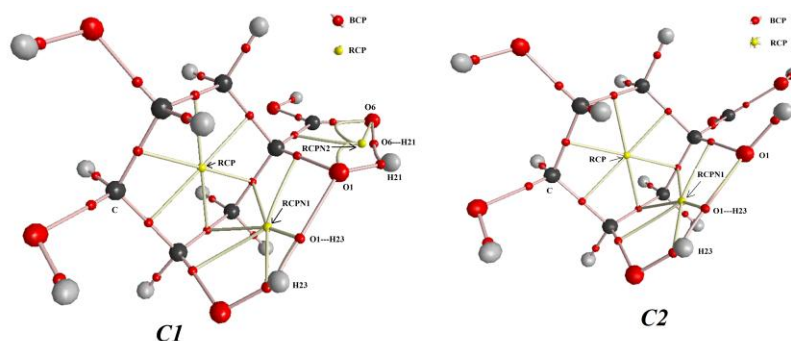
Fig 5. Details of the molecular models for the *C1* and *C2* isomers of quinic acid in gas phase showing the geometry of all their BCPs and RCPs at the B3LYP/6-311++G** level of theory.

3.5. Frontier orbitals and quantum global descriptors

To predict the reactivity and behaviours of both isomers of quinic acid in aqueous solution is very important taking into account that it acid is the main constituent of beverages, such as tea or coffee [2,23], and that some of its derivatives can be used as biopesticides, pharmaceuticals, industrial, antioxidant and anti-carcinogens agents [31,32]. Consequently, the gap energies and chemical potential (μ), electronegativity (χ), global hardness (η), global softness (S), global electrophilicity index (ω) and global nucleophilicity index (E) descriptors [33-35] were computed from the Highest Occupied Molecular Orbital (HOMO) and the Lowest Unoccupied Molecular Orbital (LUMO) by using B3LYP/6-311++G** level of theory. Thus, in **Table 8** can be observed all those properties in both media together with the equations used to calculate the descriptors. Observing the gaps results, *C1* is clearly most

Citation: Silvia Antonia Brandán et al. Ijsrm.Human, 2018; Vol. 11 (1): 25-56.

40

reactive than *C2* in both media justifying its higher solvation energy and volume expansion in solution while the higher global softness and hardness are predicted for *C1* and *C2*, respectively, as expected due to their gap values.

Table 8. The frontier molecular HOMO and LUMO orbitals and some descriptors for the *C1* and *C2* forms of quinic acid in gas and aqueous solution phases and by using the B3LYP/6-311++G** method.

B3LYP/6-311++G** Method				
	C1		*C2*	
(eV)	Gas	PCM	Gas	PCM
HOMO	-7.2507	-7.2731	-7.3008	-7.3933
LUMO	-1.0854	-0.8339	-1.0098	-0.8490
GAP	6.1653	6.4392	6.291	6.5443
DESCRIPTORS				
(eV)	Gas	PCM	Gas	PCM
χ	-3.0827	-3.2196	-3.1455	-3.2722
μ	-4.1681	-4.0535	-4.1553	-4.1212
η	3.0827	3.2196	3.1455	3.2722
S	0.1622	0.1553	0.1590	0.1528
ω	2.8178	2.5517	2.7446	2.5952
E	-12.8486	-13.0506	-13.0705	-13.4850

[a]This work

χ = - [E(LUMO)- E(HOMO)]/2 ; μ = [E(LUMO) + E(HOMO)]/2; η = [E(LUMO) - E(HOMO)]/2;

S = ½η; ω = μ^2/2η; E=$\mu*\eta$

In relation to the electrophilicity indexes, the higher values are observed for *C1* in gas phase while *C2* present the higher nucleophilicity indexes in both media. These differences in electrophilicity and nucleophilicity indexes for *C1* and *C2*, respectively could easily justify their respective strong red and blue colorations observed in the mapped surfaces, as shown in Figure 4.

3.6. NMR study

The predicted ^{1}H and ^{13}C NMR chemical shifts for *C1* and *C2* of quinic acid in aqueous solution calculated by using the GIAO method [54] are shown in **Tables 9** and **10**, respectively where the RMSD values are used to compare these values with the corresponding experimental ones in DMSO-d$_6$ and D$_2$O solutions [39-41]. Analyzing first the

Citation: Silvia Antonia Brandán et al. Ijsrm.Human, 2018; Vol. 11 (1): 25-56.

41

predicted ^{1}H-NMR chemical shifts for *C1* and *C2* a better concordance it is observed when the values are compared with those taken from Ref [39] (0.3 and 0.2 ppm) probably because in this case the ^{1}H nucleus corresponding to the -OH groups were not predicted while if the comparisons are performed with the corresponding to Ref [40] the RMSD values slightly increase for both forms to 2.9 and 2.6 ppm. Here, the differences could be in part also attributed to the calculations because they were performed in aqueous solution. For the ^{13}C nucleus the better correlations are observed by using the Ref [39] (4.5 and 3.4 ppm) probably due to same reasons explained before for H nucleus. In general, the predicted values for both ^{1}H and ^{13}C nucleus are in reasonable concordance with the experimental ones taking into account the solvent used.

Table 9. Observed and calculated ^{1}H chemical shifts (δ in ppm) for *C1* and *C2* of quinic acid in aqueous solution by using the B3LYP/6-311++G** levels of theory.

δ (ppm)	B3LYP		Exp[b]	Exp[c]
	C1	*C2*		
14-H	2.03	2.03	2.038	1.880
15-H	1.37	1.79	1.95	1.719
16-H	2.11	2.17	1.863	1.870
17-H	1.95	2.05	2.038	1.759
18-H	4.19	3.69	4.131	3.758
19-H	3.57	3.86	4.008	3.891
20-H	3.55	3.14	3.538	3.254
21-H	1.13	0.94		5.40
22-H	0.07	1.96		4.60
23-H	3.02	2.84		5.40
24-H	0.10	1.64		4.60
25-H	5.85	5.91		12.0
RMSD[b]	**0.3**	**0.2**		
RMSD[c]	**2.9**	**2.6**		

[a]This work, [b]From Ref [39], [c]From Ref [40] in DMSO-d*6*.

Citation: Silvia Antonia Brandán et al. Ijsrm.Human, 2018; Vol. 11 (1): 25-56.

42

Table 10. Observed and calculated ^{13}C chemical shifts (δ in ppm) for *C1* and *C2* of quinic acid in aqueous solution by using the B3LYP/6-311++G levels of theory.**

δ (ppm)	B3LYP/6311++G**Metho		Exp[b]	Exp[c]
	C1	*C2*		
7-C	82.86	84.47	79.7362	76.37
8-C	49.28	45.16	43.4153	37.51
9-C	38.50	39.65	40.1100	40.99
10-C	70.70	73.03	73.1506	70.78
11-C	78.38	76.13	69.7127	67.12
12-C	80.67	81.33	77.9417	75.61
13-C	181.41	182.12	184.1580	178.38
RMSD	**4.5**	**3.4**		
RMSD	**7.1**	**6.1**		

[a]This work, [b]From Ref [39] in D_2O, [c]From Ref [41] in D_2O.

Now, the improved results observed for both nucleus of *C2* in relation to *C1* could also support its presence in solution, as evidenced by their higher solvation energy in aqueous solution. The certain presence of *C2* in liquid phase could also suggest that this form will be present in the solid state.

4. Vibrational study

In this study, only *C2* was considered because this isomer was experimentally found in the solid phase [3] and is the *Cis* structure present in natural products. The structures in both media were optimized with C_1 symmetries by using the B3LYP/6-311++G** method and the expected 69 normal vibration modes present activities in the infrared and Raman spectra. As mentioned in section 2.1 the experimental available FTIR and FT-Raman spectra of quinic acid in the solid phase were taken from Refs [36] and [37], respectively. The comparisons between the experimental FTIR and FT-Raman spectra with the corresponding predicted for *C2* are shown in **Fig 6** and **7**, respectively.

Citation: Silvia Antonia Brandán et al. Ijsrm.Human, 2018; Vol. 11 (1): 25-56.

43
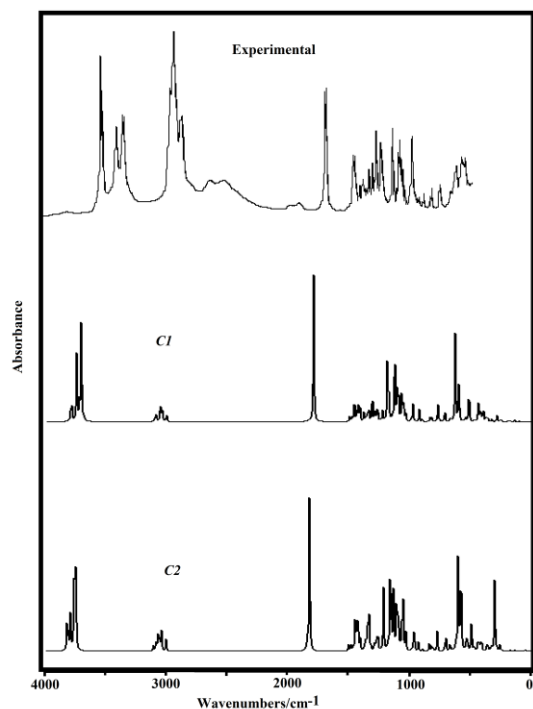
Fig 6. Comparisons between the predicted FTIR spectra for *C1* and *C2* isomers of quinic acid in gas phase at B3LYP/6-311++G** level of theory with the corresponding experimental in the solid state taken from Ref [36].
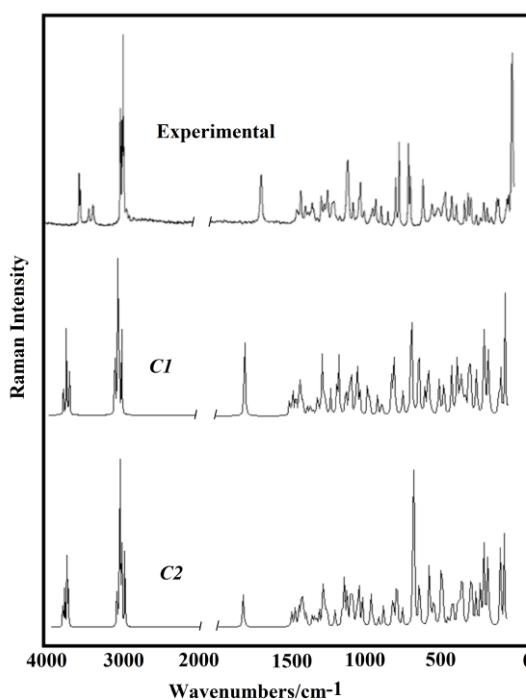
Fig 7. Comparisons between the predicted FTRaman spectra for *C1* and *C2* isomers of quinic acid in gas phase by using the B3LYP/6-311++G** level of theory with the corresponding experimental in the solid state taken from Ref [37].

In the higher wavenumbers regions, both spectra show two intense group of bands between 4000 and 2900 cm^{-1} where, obviously the first group of these bands are associated to -OH stretching modes of hydroxyl and carboxy groups and the second ones to -CH$_2$ stretching modes which are not predicted by the calculations with the same intensities. Besides, weak IR bands between 2700 and 2300 cm^{-1} are also observed which can be easily attributed to the H bonds formed by the packing forces in the crystalline solid, as was experimentally reported for this acid by Abell *et al* [3] and, by other authors for compounds containing similar groups [56-60]. Then, the differences observed between those spectra can be justified by the calculations because they were performed in the gas phase without taking into account the packing forces. **Fig 8** shows the experimental IR of quinic acid compared with those obtained for two dimeric structures presented in the same figure. It is observed that the intense bands

Citation: Silvia Antonia Brandán et al. Ijsrm.Human, 2018; Vol. 11 (1): 25-56.

44

in the higher wavenumbers region can be clearly attributed to the presence of these dimeric species, as reported by Abell *et al* [3]. On the other hand, the predicted Raman spectra in both media in activities were corrected to intensities, as suggested in the literature [61-62]. **Table 11** shows observed and calculated wavenumbers and assignments for *C2* of quinic acid in gas phase and in aqueous solution. This table shows that in solution, some vibration modes are shifted toward higher or lower wavenumbers as a consequence of the hydration of -OH groups. The vibrational assignments for *C2* were carry out considering PED contributions $\geq$ 10 %, the corresponding harmonic force fields computed with the SMQFF procedure [28] and using the Molvib program [30] and, using scale factors reported by Rauhut and Pulay [29]. Some assignments are discussed below taking into account the most important regions.

4.1. 4000-2800 cm⁻¹ region. The vibration modes corresponding to five -OH stretching modes of hydroxyl and carboxy, -CH₂ and -CH groups are expected in this region. Therefore, the IR bands observed from 3532 to 3344 cm⁻¹ are easily attributed to -OH stretching modes while the Raman bands at 2971 and 2964 cm⁻¹ are assigned to the two antisymmetric -CH₂ stretching modes. Note that in solution the -OH stretching modes are predicted shifted toward lower wavenumbers due to the hydrations of these groups by water molecules. Here, the intense Raman bands at 2934 and 2919 cm⁻¹ are easily attributed to the expected symmetric -CH₂ stretching modes. In *C2*, the three -CH stretching modes are assigned to the IR and Raman bands between 2948 and 2856 cm⁻¹, as predicted by SQM calculations.

Table 11. **Observed and calculated wavenumbers (cm⁻¹) and assignments for the *C2* form of quinic acid in gas and in aqueous solution phases.**

Experimental		B3LYP/6-311++G** Method[a]			
		GAS		PCM	
IR[c]	Raman[d]	SQM[b]	Assignments[a]	SQM[b]	Assignments[a]
3532s	3528w	3656	νO1-H21	3628	νO2-H22
3515s	3513w	3634	νO2-H22	3621	νO1-H21
3399m		3605	νO5-H25	3592	νO4-H24
3357sh		3595	νO4-H24	3554	νO5-H25
3344m		3587	νO3-H23	3548	νO3-H23
	2971s	2978	νₐCH₂(C9)	2983	νₐCH₂(C9)
2960s	2964m	2955	νₐCH₂(C8)	2968	νₐCH₂(C8)
	2948s	2939	νC11-H19	2952	νC11-H19
2927vs	2934vs	2929	νₛCH₂(C9)	2937	νC12-H20
2919sh	2919m	2916	νₛCH₂(C8)	2933	νₛCH₂(C9)
2919sh	2919m	2912	νC12-H20	2915	νₛCH₂(C8)
2856m		2875	νC10-H18	2889	νC10-H18

Citation: Silvia Antonia Brandán et al. Ijsrm.Human, 2018; Vol. 11 (1): 25-56.

45

1681s	1682w	1752	νC13=O6	1685	νC13=O6
1450m		1431	δCH₂(C1)	1429	δCH₂(C1)
1428w	1434w	1410	δCH₂(C5)	1410	δCH₂(C5)
1400w	1406w	1393	ρC11H19	1392	ρC11H19
1400w	1406w	1386	ρ'C10H18	1382	ρC12H20
1384sh		1383	ρC10H18	1372	ρC10H18
1378w		1376	wag CH₂(C5)	1367	ρ'C10H18
1359w	1352w	1360	ρC12H20	1352	wag CH₂(C5)
1345w		1319	ρ'C11H19ρCH₂(C5)	1322	νC7-C13
1326w		1308	wag CH₂(C1)	1314	ρCH₂(C5)δO1-
1294w	1306w	1293	wag CH₂(C1)	1302	wag CH₂(C1)
1271m	1288w	1287	δO1-H21ρCH₂(C1)	1294	δO1-H21
	1266w	1275	ρ'C12H20ρCH₂(C5)	1273	ρCH₂(C5)
1230m		1252	ρ'C12H20	1251	ρ'C11H19
1230m		1226	δO3-H23	1226	δO3-H23
1222sh		1216	δO2-H22	1216	δO2-H22
	1199m	1211	δO4-H24	1208	δO4-H24
	1199m	1165	ρCH₂(C1)	1158	ρCH₂(C1)
1134m	1139w	1107	δO5-H25	1135	δO5-H25νC13-O5
1126sh		1098	δO1-H21 νC7-C9	1085	δO1-H21νC7-C8
1101w	1106w	1077	νC11-O3	1072	τR₁(A1)νC7-O1
1078m		1064	νC10-O2 βR₁(A1)	1052	νC10-O2
1063m	1059w	1049	νC12-O4	1039	νC12-O4νC8-C10
1050w	1059w	1028	νC9-C11	1024	νC12-O4νC9-C11
1029w		1013	νC8-C10	1006	νC8-C10
988sh		992	νC11-O3 νC7-C8	991	νC7-C8
976s	964w	935	νC7-O1	934	νC7-O1
922w	929w	921	νC13-O5 νC7-C13	932	νC9-C11νC7-O1
880w		874	τwCH₂(C1)	871	νC11-
833w	838w	829	τwCH₂(C5) νC11-	830	τwCH₂(C5)νC11-
814w	817m	791	νC11-	789	νC11-O3
752sh	767m	775	νC7-C8	780	τwCH₂(C1)
746w	745w	748	γCOO	746	γCOO νC7-C9
659w	665w	679	δCOO	688	δCOO
611m	609w	648	δO3C11C12νC10-	647	δO3C11C12νC10-
567m		580	δCOOδO3C11C9	591	τO5-H25
550sh		533	τO5-H25	583	τO5-
538m	526w	520	δO4C12C10	540	τO3-H23
538m	526w	511	ρCOO	522	δO4C12C10ρCOO
510w		507	τO4-H24	512	ρCOO
	465w	450	δO2C10C8	458	δO2C10C8
	455w	434	τO3-H23	443	τO4-H24
	404w	411	δO2C10C12	413	δO2C10C12ρC7-
	404w	390	δO3C11C9	395	ρ'C7-O1
	383w	376	τO2-H22	373	τO2-H22
	367w	349	ρC7-O1	354	βR₂(A1)
	367w	340	ρ'C7-O1	349	ρCOO τR₁(A1)
		317	βR₃(A1)	328	τO1-H21δO3C11C9

Citation: Silvia Antonia Brandán et al. Ijsrm.Human, 2018; Vol. 11 (1): 25-56.

46

283w	274	τO1-	304	βR₃(A1)
283w	263	τO1-H21	271	δO4C12C10
262w	244	δO2C10C12	247	τR₁(A1)
202w	236	δO4C12C11	232	δO4C12C11
191w	163	τR₁(A1)δC8C7C13	177	τR₃(A1)
137w	157	τR₃(A1)δC9C7C13	171	δC9C7C13
127w	127	τR₃(A1)τR₂(A1)	134	τR₃(A1)τR₂(A1)
106m	84	τR₂(A1)	94	τR₂(A1)
	38	τCOO	30	τCOO

Abbreviations: ν, stretching; δ, deformation in the plane; γ, deformation out of plane; wag, wagging; τ, torsion; βR, deformation ring τR, torsion ring; ρ, rocking; τw, twisting; δ, deformation; a, antisymmetric; s, symmetric; (A1), Ring 1; [a]This work, [b]From scaled quantum mechanics force field, [c]From Ref [36], [d]From Ref [37].
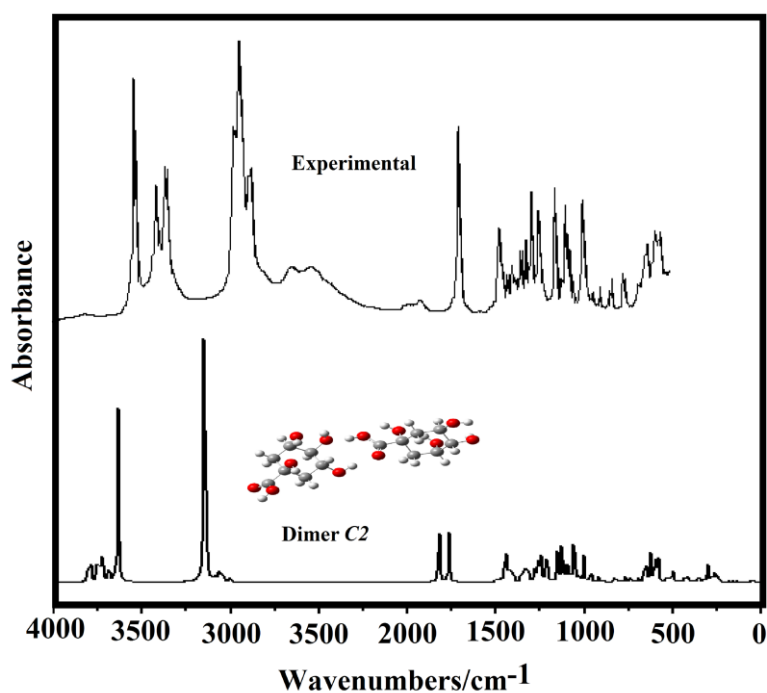
Fig 8. Comparisons between the predicted FTIR spectra for dimer *C2* of quinic acid in gas phase by using the B3LYP/6-311++G level of theory with the corresponding experimental in the solid state taken from Ref [36].**

4.2. 1700-1000 cm^{-1} region. In this region are expected the C=O, C-O and C-C stretching modes, -OH and -CH$_2$ deformations, -CH$_2$ wagging and rocking -CH modes. Accordingly, the strong IR at 1681 cm^{-1} is clearly assigned to the C13=O6 stretching modes while the IR bands of media intensities at 1078 and 1063 cm^{-1} are assigned to C-O stretching modes. Here,

Citation: Silvia Antonia Brandán et al. Ijsrm.Human, 2018; Vol. 11 (1): 25-56.

47

the intensity of this band is clearly increased due to the dimeric species because in *C2* this band it is observed with low intensity. The IR bands at 1450 and 1428 cm^{-1} are assigned to the two -CH$_2$ deformations modes while between 1400 and 1230 cm^{-1} are predicted the -CH$_2$ wagging and rocking -CH$_2$ and -CH modes and, for these reasons, these modes are assigned in these regions, as detailed in Table 11. The -OH deformations are predicted by SQM calculations between 1287 and 1095 cm^{-1} and, as was also observed in other similar species [33,56-60], and hence, they are assigned accordingly.

In this region are also predicted at 1074 cm^{-1} a deformation ring mode (β_R) in gas phase while the corresponding torsion ring mode (τ_R) in solution is predicted at 1072 cm^{-1}. Therefore, the IR bands at 1101 and 1078 cm^{-1} are associated to these vibration modes.

4.3. 1000-100 cm^{-1} region. Vibration modes related to C-O and C-C stretching modes, to carboxyl group and other to -O-H torsions, -CH$_2$ twisting modes and deformations (β_R) and torsion (τ_R) modes corresponding to the cyclohexane ring are expected in this region. The assignments of all modes located in that region were performed considering the assignments for species with similar groups [33,56-60], as shown in Table 11. Here, it is necessary to clarify that all -OH torsion modes are predicted by calculations in gas phase at different wavenumbers than in aqueous solution as a consequence of hydration of these groups with water molecules, as supported by AIM studies due to the formation of O1---H23 interactions in both media (Table 7).

5. Force constants

Force constants are very important properties to analyze particularly the forces of different bonds and, in the quinic acid, the evaluations of these constants for *C1* and C2 are of interest taking into account the different positions in their structures of the carboxyl OH groups. Thus, the harmonic force fields expressed in Cartesian coordinates and computed with the SMQFF approach [28] and the Molvib program [30] at B3LYP/6-311++G** level of theory were transformed to normal internal coordinates with the Molvib program by using scale factors [29,30]. Hence, the scaled internal force constants were obtained for those two isomers. The results can be seen in **Table 12** compared with the most stable species of carquejyl acetate in both media [63] and with the two conformers of (5,7-Dichloro-quinolin-8-yloxy) acetic acid in gas phase [64] in order to see as change the values when other groups are present in their structures.

Citation: Silvia Antonia Brandán et al. Ijsrm.Human, 2018; Vol. 11 (1): 25-56.

48

Table 12. Scaled internal force constants for *C1* and *C2* of quinic acid in gas and aqueous solution phases.

B3LYP/6-311++G** Method[a]				Carquejyl acetate[b]		(5,7-Dichloro-quinolin-8-yloxy)	
Force constan	*C1*		*C2*				*C1*	*C2*
	Gas	PCM	Gas	PCM	Gas	PCM	*C1*	*C2*
$f(\nu O$-	7.25	7.08	7.32	7.08			6.10	7.73
$f(\nu O$-	7.21	7.29	7.28	7.24				
$f(\nu C=O$	11.93	11.45	12.3	11.36	11.90	11.30	13.65	14.22
$f(\nu C$-	5.82	5.86	5.29	5.87	4.55	4.45	6.36	6.08
$f(\nu C$-	4.68	4.43	4.63	4.43				
$f(\nu CH_2)$	4.79	4.79	4.78	4.80	5.05	4.91	5.34	5.29
$f(\nu C$-H)	4.66	4.66	4.66	4.72	4.85	4.85	5.69	5.67
$f(\nu C$-	3.78	3.80	3.80	3.82	4.02	4.08		
$f(\nu C$-C)	3.82	3.58	3.65	3.60				
$f(\delta O$-	0.66	0.66	0.64	0.66				
$f(\delta O$-	0.75	0.74	0.73	0.74			1.06	0.79
$f(\delta COO$	1.31	1.31	1.31	1.32	1.30	1.30	1.34	1.23
$f(\delta CH_2)$	0.69	0.69	0.70	0.70	0.40	0.40	0.91	0.83

Units are mdyn Å^{-1} for stretching and mdyn Å rad^{-2} for angle deformations

[a]This work, [b]From Ref. [63], [c]From Ref. [64]

The exhaustive initial inspection of that table shows that the main differences between the force constants are related to the different positions of carboxyl OH groups in *C1* and *C2*. Therefore, evaluating the $f(\nu O$-H$)_C$ force constant values of carboxyl OH groups, the higher value observed for *C2* in gas phase could be attributed to the higher value of the $LP(2)O5 \rightarrow \pi^*O6$-C13 interaction in *C1* where the O5 atom is involved in the carboxyl O-H bond. Probably, for this reason, the bond order value observed from Table 5 for the O5 atom in *C1* in that medium is higher than *C2*. Hence, the $f(\nu O$-H$)_C$ force constant in gas phase is higher in *C2* than *C1*, however, in solution, the same values are observed for both forms. A different result it is observed when the $f(\nu O$-H$)_H$ force constant values of hydroxy groups are analyzed. The higher $f(\nu C=O)$ force constant value for *C2* in gas phase than *C1* can be justified because the O6 atom of C=O bond is free in *C2* while in *C1* is involved in the O6---H21 bond. The higher $f(\nu C$-O$)_C$ force constant value for *C1* than C2 can be justified by the higher value of the $LP(2)O5 \rightarrow \pi^*O6$-C13 interaction because in *C1* the O5 atom is involved in the carboxyl O-H bond. The other constants present similar values in *C1* and *C2*. If the force constants of quinic acid are compared with those observed for carquejyl acetate in both media [63] there are differences that could be easily explained by the presence in carquejyl acetate of an

Citation: Silvia Antonia Brandán et al. Ijsrm.Human, 2018; Vol. 11 (1): 25-56.

49

acetate, two =CH$_2$ groups and one C=C bond in the six members ring. When the force constants are compared with those reported for two conformers of (5,7-dichloro-quinolin-8-yloxy) acetic acid in gas phase [64] it is observed higher values in practically all force constants of this acid possibly due to that in 5,7-dichloro-quinolin-8-yloxy group is linked to acetic acid. In this acid, the low value observed in $f(\nu O\text{-}H)_C$ of *C1* is connected directly with the H bond formed between the H atom of carboxy group with the O atom of quinolin ring while in *C2* there is not H bond formation.

6. Ultraviolet-visible spectrum

In **Fig 9** are given the predicted ultraviolet spectra of *C1* and *C2* of quinic acid in aqueous solution by using the B3LYP/6-311++G** method compared with the corresponding experimental available taken from Rogoff and Reuter [1,65].
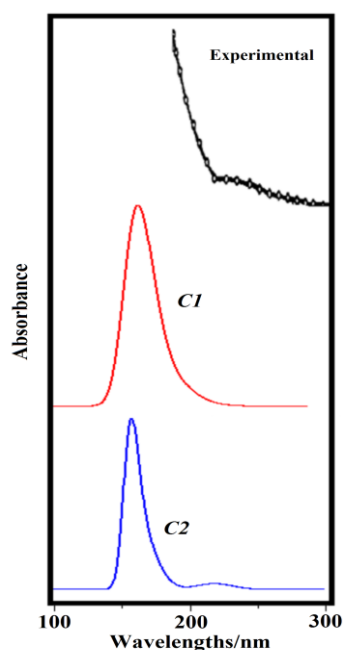
Fig 9. Comparisons between the predicted Ultraviolet spectra for *C1* and *C2* isomers of quinic acid in aqueous solution by using the B3LYP/6-311++G level of theory with the corresponding experimental in mixed of ethanol and water taken from Ref [1].**

The predicted UV spectrum for *C1* shows one intense band at 193.25 nm while the UV spectrum of *C2* predicted an intense band at 183 nm and a shoulder in c.a. 220 nm. In the experimental UV spectrum recorded in a mixed of ethanol in water solution between 220 and 300 nm is observed a shoulder in c.a. 220 nm and a weak band at 250 nm. These bands are

Citation: Silvia Antonia Brandán et al. Ijsrm.Human, 2018; Vol. 11 (1): 25-56.

50

evidently associated to $n{\rightarrow}\pi^*$ interactions (*LP(2)O$\rightarrow\pi^*$O-C*) predicted by NBO analyses, as shown in Table 6 and, as was reported for carquejol [59]. Many UV spectroscopy studies show visibly that the position of absorption maximum in quinic acid is highly dependent of used solvent and, of course, of material or substance where the quinic acid is found, for instance, in caffeine [66], sweet potato roots [67] or species related to *3-0*-caffeoylquinic acid [22] some bands of acid are shifthed.

7. Electronic circular dichroism (ECD)

The predicted ECD spectra for both *C1* and *C2* isomers of quinic acid in aqueous solution by using the B3LYP/6-311++G** method can be seen in **Fig 10.b** compared with the experimental available ECD spectrum for chlorogenic acid, 3'-O-caffeoyl D-quinic acid between 200 and 260 nm taken from Ref [68] (**Fig. 10.a**) and, with the experimental available ECD spectrum for Pr^{3+} metal ion-D-(-)-quinic acid 1:1 complex between 350 and 600 nm taken from Ref [38] (**Fig. 10.c**).
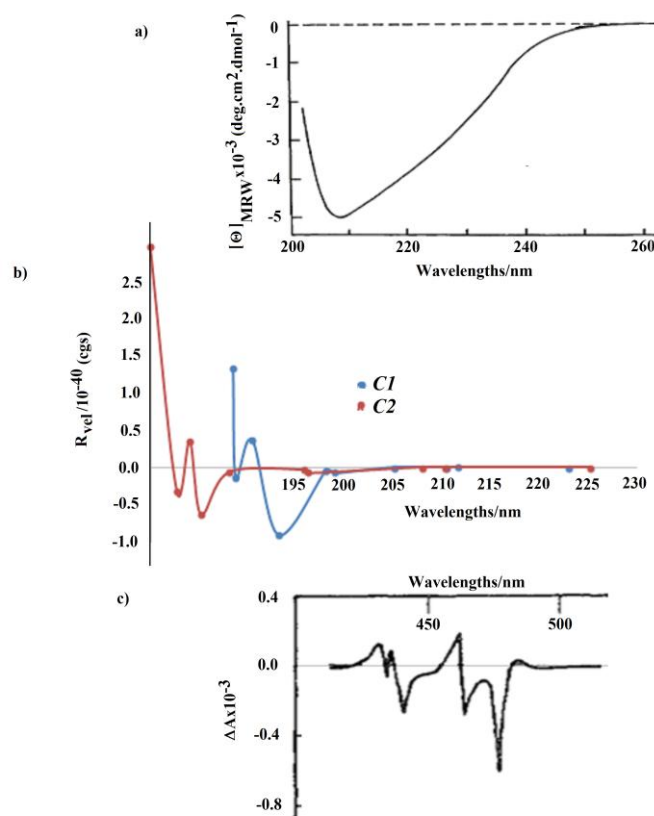
Figure 10. Predicted Rotatory Strengths in cgs (10^{-40} erg-esu-cm/Gauss) for *C1* and *C2* isomers of quinic acid in aqueous solution by using the B3LYP/6-311++G level of theory compared with the experimental ECD spectra for similar species taken from Refs [38,68].**

Citation: Silvia Antonia Brandán et al. Ijsrm.Human, 2018; Vol. 11 (1): 25-56.

51

The calculated rotatory strengths for *C1* and *C2* were simulated into an ECD curve by using the Gaussian function, as suggested by Ding *et al.* [69]. Here, when the experimental ECD spectra for p-coumaroylquinic acids obtained between 200 and 380 nm [70] are compared with those predicted here for quinic acid clearly it is evidenced that other groups have influence on the positions of bands. Theoretically, *C1* and *C2* show two negative bands due to the two asymmetric C atoms (here, C10 and C11) for which both ECD spectra are similar to corresponding to chlorogenic acid (Fig. 10.a). In the latter acid the first band it is not observed because the experimental spectrum was recorded from 200 to 260 nm [68]. The forms and number of bands are in good agreement with the spectrum obtained for the Pr^{3+} complex in Fig. 10.c. which show bands at 443.5, 469, 482 and 590 nm. Here, the two $n \rightarrow \pi^*$ interactions predicted by NBO studies are clearly observed in the ECD spectrum of both isomers despite these interactions have higher energies in *C1*. Hence, the similar behaviour between the experimental ECD spectrum from Fig. 10.c with those predicted by calculations could indicate that both isomers have the same absolute configuration of the chiral centers, confirming their absolute configuration as (3R,5R), here (11R,10R), in accordance to that structure reported for quinic acid by Abell *et al* [3]. Probably, both isomers are present in an aqueous solution.

8. CONCLUSIONS

The quinic acid was completely characterized by using the experimental available FTIR, FT-Raman, ^{1}H- and ^{13}C-NMR, ultraviolet and ECD spectroscopies. Theoretically, two isomeric structures of quinic acid, named *C1* and *C2* were studied in gas phase and in aqueous solution by using the B3LYP/6-311++G** calculations, where the positions of carboxyl OH are *Trans* and *Cis*, respectively. *C1* is most stable in gas phase but *C2* is most stable in solution showing this latter isomer low solvation energy in aqueous solution. This difference could be attributed to the low volume expansion observed for *C2*, in relation to *C1*. The dipole moment values of both isomers decrease in solution. Different behaviours between both isomers were found studying Mulliken, MK and NPA charges while the unlike nucleophilic and electrophilic sites observed for both isomers could explain different hydrations of both isomers in solution. The NBO and AIM studies could not explain the presence of *C2* in the solid phase because C1 shows a higher stability in both media. The frontier orbitals analyses reveal that *C1* is clearly most reactive than *C2* in both media justifying its higher solvation energy and volume expansion in solution while the differences in electrophilicity and

Citation: Silvia Antonia Brandán et al. Ijsrm.Human, 2018; Vol. 11 (1): 25-56.

52

nucleophilicity indexes for *C1* and *C2*, respectively could easily justify their respective strong red and blue colorations observed in the mapped surfaces. Although very good correlations are observed for *C2* in both ^{1}H- and ^{13}C-NMR spectra its presence in the quinic acid only could be supported by the ultraviolet because better correlations are observed for this isomer while the presence of both isomers could be supported by their ECD spectra. Here, for *C2* are reported for first time, the force fields, complete vibrational assignments and force constants in both media.

ACKNOWLEDGEMENTS.

REFERENCES

[1] Rogoff MH, An Aromatic Intermediate in the Bacterial Oxidation of Quinic Acid. J. Gen. Microbial. 1958; 19: 330-339.

[2] Sakata K, Sakuraba S, Yagi A, Ina K, T. Hara, Takeo T, Isolation and Identification of (–)- Quinic Acid as an Unidentified Major Tea-component, Agric. Bioi. Chern. 1986; 50 (7): 1919-1921.

[3] Abell C, Allen FH, Bugg TDH, Doyle MJ, Raithby PR, Structure of (-)-Quinic Acid, Acta Cryst. 1988; C44: 1287-1290.

[4] Flores-Parra A, Gutiérrez-Avella DM, Contreras R, Khuong-Huu F, ^{13}C and ^{1}H NMR investigations of quinic acid derivatives: Complete spectral assignment and elucidation of preferred conformations, MRC 1989; 27(6): 544-555.

[5] Shing TKM, Tang Y, (−)-Quinic acid in organic synthesis. 2. Facile syntheses of pseudo-β-D-mannopyranose and pseudo-β-D-fructopyranose, Tetrahedron, 1991; 47(26): 4571-4578.

[6] Merfort I, Caffeoylquinic acids from flowers of *Arnica montana* and *Arnica chamissonis*, Phytochemistry, 1992; 31(6): 2111-2113.

[7] Bkouche-Waksman I, Structure and Absolute Configuration of a Quinic Acid-Copper(II) Complex, Acta Cryst. 1994; C50: 62-64.

[8] Chuda Y, Ono H, Ohnishi-Kameyama M, Nagata T, Tsushida T, Structural Identification of Two Antioxidant Quinic Acid Derivatives from Garland (*Chrysanthemum coronarium* L.), J. Agric. Food Chem. 1996; 44 (8): 2037–2039.

[9] Basnet P, Matsushige K, Hase K, Kadota S, Namba T, Four di-*O*-caffeoyl quinic acid derivatives from Propolis. Potent hepatoprotective activity in experimental liver injury models, Biol. Pharm. Bull. 1996; 19(11): 1479-1484.

[10] Yue J-M, Zhao Q-S, Lin Z-W, Sun H-D, Phenolic compounds from Erigeron Breviscapus (Compositae), Acta Botanica Sinica, 2000; 42(3): 311-315.

[11] Allegretti Y, Ferrer EG, González Baró AC, Williams PAM, Oxovanadium(IV) complexes of quinic acid. Synthesis, characterization and potentiometric study, Polyhedron 2000; 19: 2613–2619.

[12] Gabriel C, Menelaou M, Daskalakis M, Lakatos A, Kiss T, Mateescu C, Raptis RG, Zoumpoulakis P, Salifoglou A, Synthetic, structural, spectroscopic and solution speciation studies of the binary Al(III)–quinic acid system. Relevance of soluble Al(III)–hydroxycarboxylate species to molecular toxicity, Polyhedron 2008; 27: 2911–2920.

Citation: Silvia Antonia Brandán et al. Ijsrm.Human, 2018; Vol. 11 (1): 25-56.

53

[13] Pero RW, Lund H, Leanderson T, Antioxidant metabolism induced by quinic acid. Increased urinary excretion of tryptophan and nicotinamide, Phytotherapy Research, 2009; 23(3): 335-346.

[14] Zeng K, Thompson KE, Yates CR, Miller DD, Synthesis and biological evaluation of quinic acid derivatives as anti-inflammatory agents. Bioorganic & medicinal chemistry letters. 2009; 19(18): 5458-5460.

[15] Parveen I, Threadgill MD, Hauck B, Donnison I, Winters A, Isolation, identification and quantitation of hydroxycinnamic acid conjugates, potential platform chemicals, in the leaves and stems of *Miscanthus-giganteus* using LC–ESI-MSn, Phytochemistry 2011; 72: 2376–2384.

[16] El-Abassy RM, Donfack P, Materny A, Discrimination between Arabica and Robusta green coffee using visible micro Raman spectroscopy and chemometric analysis, Food Chemistry 2011; 126: 1443–1448.

[17] Abu-Reidah IM, Arraez-Roman D, Segura-Carretero A, Fernandez-Gutierrez A, Extensive characterisation of bioactive phenolic constituents from globe artichoke (*Cynara scolymus L.*) by HPLC–DAD-ESI-QTOF-MS, Food Chemistry 2013; 141: 2269–2277.

[18] Zhang Q, Jiang Y, Toutounchian J, Wilson MW, Morales-Tirado V, Miller DD, et al. Novel quinic acid derivative KZ-41 prevents retinal endothelial cell apoptosis without inhibiting retinoblastoma cell death through p38 signaling. Invest Ophthalmol Vis Sci. 2013; 54(9):5937-5943.

[19] Toutounchian JJ, Steinle JJ, Makena PS, Waters CM, Wilson MW, Haik BG, et al. Modulation of radiation injury response in retinal endothelial cells by quinic acid derivative KZ-41 involves p38 MAPK. PloS one. 2014; 9(6): e100210.

[20] He H, Weir RL, Toutounchian JJ Pagadala J, Steinle JJ, Baudry J, Miller DD, Yates CR, The quinic acid derivative KZ-41 prevents glucose-induced caspase-3 activation in retinal endothelial cells through an IGF-1 receptor dependent mechanism, PLOS ONE, https://doi.org/10.1371/journal.pone.0180808 August 10, 2017.

[21] Pomenta JV, Burns EE, factors affecting chlorogenic, quinic and caffeic acid levels in sunflower kernels, J. Food Science, 1971; 36: 490-492.

[22] Hanson KR, Zucker M, The Biosynthesis of Chlorogenic Acid and Related Conjugates of the Hydroxycinnamic Acids, J. Biological Chemistry 1963; 238(3): 1105-1115.

[23] Matei MF, Jaiswal R, Kuhnert N, Investigating the Chemical Changes of Chlorogenic Acids during Coffee Brewing: Conjugate Addition of Water to the Olefinic Moiety of Chlorogenic Acids and Their Quinides, J. Agric. Food Chem., 2012; 60(49): 12105-12115.

[24] Jaiswal R, Dickman MH, Kuhnert N, First diastereoselective synthesis of methyl caffeoyl- and feruloyl-muco-quinates, Org. Biomol. Chem. 2012; 27(10): 5266-5277.

[25] Hanson KR, Chlorogenic acid biosynthesis, Phytochemistry, 1966; 5: 491-499.

[26] Sefkow M, First Efficient Synthesis of Chlorogenic Acid, European J. Org. Chem. 200; 1(6): 1137-1141

[27] da Encarnação JA, Farrell TL, Ryder A, Kraut NU, Williamson G, In vitro enzymic hydrolysis of chlorogenic acids in coffee, Molecular Nutrition and Food Research, 2015; 59 (2): 231-239.

[28] Pulay, P.; Fogarasi, G.; Pongor, G.; Boggs, J. E.; Vargha, A. Combination of theoretical ab initio and experimental information to obtain reliable harmonic force constants. Scaled quantum mechanical (QM) force fields for glyoxal, acrolein, butadiene, formaldehyde, and ethylene, J. Am. Chem. Soc. 1983; 105: 7073.

[29] Rauhut G, Pulay P, Transferable Scaling Factors for Density Functional Derived Vibrational Force Fields, J. Phys. Chem. 1995; 99: 3093-3100. b) Correction: G. Rauhut, P. Pulay, J. Phys. Chem. 1995; 99: 14572.

[30] Sundius T. Scaling of ab-initio force fields by MOLVIB. Vib. Spectrosc. 2002; 29:89-95.

[31] Xiubin L, Synthesis of new dicinnamoyl quinic acid derivatives and analogs and the evaluation of their potential as biopesticides, Thesis, Ecology, environment. Université de Lyon, 2016.

[32] Gil M, Wianowska D, Chlorogenic acids – their properties, occurrence and analysis, Annales Universitatis Mariae Curie-Skłodowska Lublin – Polonia Vol. LXXII, 1 Section AA, 2017.

[33] Minteguiaga M, Dellacassa E, Iramain MA, Catalán CAN, Brandán SA, Synthesis, Spectroscopic characterization and structural study of carquejiphenol, a 2-Isopropenyl-3-methylphenol derivative with potential medicinal uses, J. Mol. Struct. 2018; 1165: 332-343.

[34] Iramain MA, Davies L, Brandán SA, FTIR, FT-Raman and UV-visible spectra of Potassium 3furoyltrifluoroborate salt, J. Mol. Struct. 2018; 1158: 245-254.

[35] Iramain MA, Davies L, Brandán SA, Evaluating structures, properties and vibrational and electronic spectra of the Potassium 2-isonicotinoyl trifluoroborate salt, J. Mol. Struct. 2018; 1163: 41-53.

[36] Available from: https://webbook.nist.gov/cgi/inchi?ID=C470633&Mask=80.htm

Citation: Silvia Antonia Brandán et al. Ijsrm.Human, 2018; Vol. 11 (1): 25-56.

54

[37] Available from: https://www.chemicalbook.com/SpectrumEN_77-95-2_Raman.htm

[38] Katzin LI, Circular dichroism of D-(-)-quinic acid and some of its metal ion complexes, Inorg. Chem. 1973; 12(8): 1951–1952.

[39] Available from Biological magnetic resonance data bank: http://www.bmrb.wisc.edu/metabolomics/mol_summary/show_data.php?molName=Quinic_acid&id=bmse0003 06&whichTab=1.htm

[40] Available from Chemical book: https://www.chemicalbook.com/SpectrumEN_77-95-2_1HNMR.htm.

[41] Available from Chemical book: https://www.chemicalbook.com/SpectrumEN_77-95-2_13CNMR.htm.

[42] Nielsen AB, Holder AJ. 2008. Gauss View 5.0, User's Reference, GAUSSIAN Inc., Pittsburgh, PA.

[43] Gaussian 09, Revision A.02, Frisch, M. J.; Trucks, G. W.; Schlegel, H. B.; Scuseria, G. E.; Robb, M. A.; Cheeseman, J. R.; Scalmani, G.; Barone, V.; Mennucci, B.; Petersson, G. A.; Nakatsuji, H.; Caricato, M.; Li, X.; Hratchian, H. P.; Izmaylov, A. F.; Bloino, J.; Zheng, G.; Sonnenberg, J. L.; Hada, M.; Ehara, M.; Toyota, K.; Fukuda, R.; Hasegawa, J.; Ishida, M.; Nakajima, T.; Honda, Y.; Kitao, O.; Nakai, H.; Vreven, T.; Montgomery, J. A., Jr.; Peralta, J. E.; Ogliaro, F.; Bearpark, M.; Heyd, J. J.; Brothers, E.; Kudin, K. N.; Staroverov, V. N.; Kobayashi, R.; Normand, J.; Raghavachari, K.; Rendell, A.; Burant, J. C.; Iyengar, S. S.; Tomasi, J.; Cossi, M.; Rega, N.; Millam, J. M.; Klene, M.; Knox, J. E.; Cross, J. B.; Bakken, V.; Adamo, C.; Jaramillo, J.; Gomperts, R.; Stratmann, R. E.; Yazyev, O.; Austin, A. J.; Cammi, R.; Pomelli, C.; Ochterski, J. W.; Martin, R. L.; Morokuma, K.; Zakrzewski, V. G.; Voth, G. A.; Salvador, P.; Dannenberg, J. J.; Dapprich, S.; Daniels, A. D.; Farkas, Ö.; Foresman, J. B.; Ortiz, J. V.; Cioslowski, J.; Fox, D. J. Gaussian, Inc., Wallingford CT, 2009.

[44] Becke AD. Density functional thermochemistry. III. The role of exact exchange. J. Chem. Phys. 1993; 98:5648-5652.

[45] Lee C, Yang W, Parr R.G. Development of the Colle-Salvetti correlation-energy formula into a functional of the electron density. Phys. Rev. 1988; B37: 785-789.

[46] Miertus S, Scrocco E, Tomasi J. Electrostatic interaction of a solute with a continuum. Chem. Phys. 1981; 55:117–129.

[47] Tomasi J, Persico J. Molecular Interactions in Solution: An Overview of Methods Based on Continous Distributions of the Solvent. Chem. Rev. 1994; 94:2027-2094.

[48] Marenich AV, Cramer CJ, Truhlar D.G. Universal solvation model based on solute electron density and a continuum model of the solvent defined by the bulk dielectric constant and atomic surface tensions. J. Phys. Chem. 2009; B113:6378-6396.

[49] Ugliengo P. MOLDRAW Program, University of Torino, Dipartimento Chimica IFM, Torino, Italy, 1998.

[50] Besler BH, Merz Jr KM, Kollman PA, Atomic charges derived from demiempirical methods, J. Comp. Chem. 1990; 11: 431-439.

[51] Glendening ED, Badenhoop JK, Reed AD, Carpenter JE, Weinhold F. 1996. NBO 3.1; Theoretical Chemistry Institute, University of Wisconsin; Madison.

[52] Biegler-Köning F, Schönbohm J, Bayles DJ. AIM2000; a program to analyze and visualize atoms in molecules. Comput. Chem. 2001; 22:545-559.

[53] Bader RFW. Atoms in Molecules. A Quantum Theory, Oxford University Press, Oxford, ISBN: 0198558651; 1990.

[54] Ditchfield R, Self-consistent perturbation theory of diamagnetism. I. A gage invariant LCAO (linear combination of atomic orbitals) method for NMR chemical shifts, Mol. Phys 1974; 27: 714-722.

[55] Bushmarinov I.S., Lyssenko K.A., Antipin M.Yu; Atomic energy in the ′ Atoms in Molecules′ theory and its use for solving chemical problems, Russian Chem. Rev. 2009; 78(4): 283-302.

[56] Chain F, Iramain MA, Grau A, Catalán CAN, Brandán SA, Evaluation of the structural, electronic, topological and vibrational properties of N-(3,4-dimethoxybenzyl)-hexadecanamide isolated from Maca (Lepidium meyenii) using different spectroscopic techniques, J. Mol. Struct. 2016; 1119: 25-38.

[57] Chain FE, Ladetto MF, Grau A, Catalán CAN, Brandán SA, Structural, electronic, topological and vibrational properties of a series of N-benzylamides derived from Maca (Lepidium meyenii) combining spectroscopic studies with ONION calculations, J. Mol. Struct. 2016; 1105: 403-414.

[58] Issaoui N, Ghalla H, Brandán SA, Bardak F, Flakus HT, Atac A, Oujia B, Experimental FTIR and FTRaman and theoretical studies on the molecular structures of monomer and dimer of 3-thiopheneacrylic acid, J. Mol. Struct. 2017; 1135: 209-221.

Citation: Silvia Antonia Brandán et al. Ijsrm.Human, 2018; Vol. 11 (1): 25-56.

55

[59] Minteguiaga M, Dellacassa E., Iramain MA, Catalán CAN., Brandán SA, A structural and spectroscopic study on carquejol, a relevant constituent of the medicinal plant Baccharis trimera (Less.) DC. (Asteraceae), J. Mol. Struct. 2017; 1150: 8-20.

[60] Iramain MA, Davies L, Brandán SA, Structural and spectroscopic differences among the Potassium 5-hydroxypentanoyltrifluoroborate salt and the furoyl and isonicotinoyl salts, J Mol. Struct. 2019; 1176: 718-728.

[61] Keresztury G, Holly S, Besenyei G, Varga J, Wang AY, Durig JR, Vibrational spectra of monothiocarbamates-II. IR and Raman spectra, vibrational assignment, conformational analysis and ab initio calculations of S-methyl-N,N-dimethylthiocarbamate, Spectrochim. Acta, 1993; 49A: 2007-2026.

[62] Michalska D, Wysokinski R, The prediction of Raman spectra of platinum(II) anticancer drugs by density functional theory, Chem. Phys Letters, 2005; 403: 211-217.

[63] Minteguiaga M, Dellacassa E, Iramain MA, Catalán CAN, Brandán SA, FT-IR, FT-Raman, UV-Vis, NMR and structural studies of Carquejyl Acetate, a component of the essential oil from *Baccharis trimera* (Less.) DC. (Asteraceae), submitted to J Mol. Struct. 2019; 1177: 499-510.

[64] Romano E, Castillo MV, Pergomet J, Zinczuk J, Brandán SA, Synthesis and structural and vibrational analysis of (5,7-dichloro-quinolin-8-yloxy) acetic acid J. Mol. Struct. 2012; 1018: 149–155.

[65] Wilhad M. Reuter, Analysis of Organic Acids in Fruit Juices by HPLC and UV Detection, Perkin Elmer, Inc. Shelton, CT, 2015.

[66] Navarra G, Moschetti M, Guarrasi V, Mangione MR, Militello V, Leone M, Simultaneous Determination of Caffeine and Chlorogenic Acids in Green Coffee by UV/Vis Spectroscopy, Journal of Chemistry, 2017; Article ID 6435086, 8 pages.

[67] Minamika T, The Occurrence of Quinic Acid in Sweet Potato Roots, Agr. Biol. Chem. 1967; 31(1): 124-.126.

[68] Suryaprakash P, Prakash V, Interaction of 3'-O-caffeoyl D-quinic acid with multisubunit protein helianthinin, J. Biosci. 1995; 20(4): 531–549.

[69] Ding Y., Li X-C, Ferreira D, Theoretical Calculation of Electronic Circular Dichroism of a Hexahydroxydiphenoyl-containing Flavanone Glycoside, J Nat Prod. 2009; 72(3): 327–335.

[70] Gutiérrez Ortiz AL, Berti F, Navarini L, Monteiro A, Resminic M, Forzato C, Synthesis of p-coumaroylquinic acids and analysis of their interconversion, 2017.

Citation: Silvia Antonia Brandán et al. Ijsrm.Human, 2018; Vol. 11 (1): 25-56.

56